



Research Article

Multi-Objective optimization of a parabolic trough solar power plant integrated with an organic Rankine cycle: based on high pressure and working fluid mass flow rate

Ömer Faruk GÜLER^a 

^aAfyon Kocatepe University, Faculty of Technology, Afyon, 03200, Turkey

ARTICLE INFO

Article history:

Received 23 September 2024

Accepted 29 January 2025

Published 23 April 2025

Keywords:

Multi-objective optimization

PTC solar energy plant

Thermoeconomic analysis

ABSTRACT

The optimization of a parabolic trough solar power plant is conducted using a multi-objective optimization algorithm in this study. Initially, the design of the plant, planned to be built in Afyonkarahisar province, is developed. Thermodynamic and thermo-economic analyses are performed based on this design. Key variables significantly affecting the system's outputs are identified as the fluid flow rate used in the Organic Rankine Cycle (ORC) and the turbine inlet pressure. A parametric study is carried out for these variables. However, optimizing the system requires more than just these parameters. The system is optimized multi-objectively, considering all relevant variables. A graphical multi-objective optimization algorithm is applied in this process. For the base case values of a 30 kg/s flow rate and 3500 kPa turbine inlet pressure, the net energy production, exergy efficiency, and unit energy cost are 0.8443 MW, 2.32%, and 0.2230 \$/kWh, respectively. After optimization, the best results are achieved at a flow rate of 42 kg/s and a pressure of 4000 kPa. For the optimized case, the net energy production, exergy efficiency, and unit energy cost improve to 1.228 MW, 3.37%, and 0.1781 \$/kWh, respectively.

1. Introduction

The importance of renewable energy is undeniable. For this reason, many organizations aim to transition to zero-emission energy production methods by the 2050s [1]. Among the many studies on renewable energy, solar energy research holds a significant share. Solar energy systems are continuously diversifying, and among them, concentrator solar energy systems are particularly important due to their high power density. Parabolic trough collectors (PTCs) are one of the most extensively studied systems in the literature.

Some studies focus on detailed designs and the development or improvement of components for energy facilities [2]. Others conduct system analyses to evaluate the most efficient configurations using designed components. To maximize energy utilization, exergy analyses are often performed to achieve maximum efficiency [3]. Optimized systems aim to determine the most efficient operating ranges to achieve the highest possible performance. However, as system complexity increases, the number of variables and outputs also grows. For instance, optimizing efficiency and energy production

in a system with a single power-producing turbine may also reduce costs. However, in more complex systems, the points where maximum efficiency and minimum cost align may differ, or a highly efficient system may fail to produce sufficient power. At this stage, algorithms capable of optimizing multiple variables simultaneously are needed [4,5]. Multi-objective optimization algorithms address this challenge by optimizing several objective functions concurrently [6]. In various studies, both basic and multi-objective optimization algorithms have been employed [7,8]. Some studies utilize complex algorithms through software packages and built-in tools [9]. For example, Desai and Bandyopadhyay [10] designed a PTC-based system without a separate storage unit. The system included a hot fluid cycle and a Rankine cycle, using variables such as turbine inlet temperature, turbine inlet pressure, design radiation, and system size. Optimization efforts resulted in a minimum energy cost of 0.188 \$/kWh. In another study [11], a more complex system was analyzed. Heat from parabolic collectors was transferred via an intermediary fluid and then stepwise into a Rankine cycle, producing energy through both high-pressure and low-pressure turbines. Using the Combined Energy-

* Corresponding author. Tel.: +90 272 218 2536

E-mail addresses: ofguler@aku.edu.tr (O.F.Guler)

ORCID: 0000-0002-3344-341X (O.F.Guler)

DOI: [10.35860/iarej.1554883](https://doi.org/10.35860/iarej.1554883)

© 2025, The Author(s). This article is licensed under the CC BY-NC 4.0 International License (<https://creativecommons.org/licenses/by-nc/4.0/>).

Exergy Control Method, which integrates energy and exergy analysis, system efficiencies of 36.06% were achieved, alongside a 25.09% improvement in system response time. After a triple optimization, energy efficiency, exergy efficiency, and response time improved to 34.02%, 28.25%, and 17.63%, respectively. Colakoğlu and Durmayaz [12] designed a complex solar energy system featuring energy production through a gas turbine and secondary utilization of the remaining energy via systems such as the Kalina Cycle and Organic Rankine Cycle (ORC). The system also provided heating and cooling. Optimization efforts enhanced the exergetic quality factor. Georgousis et al. [13] performed multi-objective optimization of a polygeneration system using a geometric approach, a method similar to the one used in this study. Modabber and Manesh [14] examined a trigeneration system incorporating a solar PTC, producing power, desalination, and heat. They analyzed parameters like unit energy cost, environmental impact, and exergy efficiency using both a multi-objective genetic algorithm and a water cycle algorithm. The latter achieved a 12.66% increase in exergy efficiency, with total operating costs of 47.4 \$/h and an environmental impact of 49.2 pts/h. Esfahani et al. [15] conducted an energy, exergy, economic, and environmental analysis of a solar energy system designed for Iran. Their study showed the highest energy efficiency in July (73.6%) and the highest exergy efficiency in January (20.11%). The lowest unit exergy cost was 70.17 \$/GJ in June, and CO₂ savings were 0.0193\$/h. Multi-objective genetic algorithm optimization improved exergy efficiency by 6.27% and reduced total system costs by 20.36%. In another study [16], a system using different heat transfer fluids in PTCs was optimized. Mixtures like aluminum oxide, MgO, TiO, and ZnO were employed, and exergy analyses were conducted for systems combined with the Kalina Cycle. Multi-objective genetic algorithm optimization determined optimal system parameters. These studies demonstrate the critical role of multi-objective optimization in energy, efficiency, and cost analyses, especially for multi-generation systems. Complex applications like ammonia and hydrogen production, pure water generation, electricity production, and heat production require even more intricate analyses. While many researchers rely on software packages, traditional methods like one-dimensional genetic algorithms and graphical techniques are still widely used.

The novelty of this study lies in the combining conventional PTC calculations and energy system integration with economic analyses, particularly multi-objective optimization algorithm. Under the conditions of Afyonkarahisar, this modeled system not only offers a regionally applicable design but also serves as a reference for other renewable energy studies through the optimization system to be implemented. For this purpose, in this study, a parabolic trough solar energy system was designed and integrated with an ORC for energy production. In addition to traditional graphical optimization methods, a normalization algorithm was applied to the graphical data, creating a unified objective

function. Energy, exergy, and economic analyses were performed to determine optimal operating conditions.

2. Method

2.1 System Description

A solar power system is being designed for implementation in Afyonkarahisar province, a region with significant solar energy potential. The system schematic is presented in Figure 1. Due to its continental climate, Afyonkarahisar experiences minimal haze, allowing abundant use of clear sunlight. According to the literature, solar irradiation values during summer range from 600 to 1000 W/m² [17]. For this study, an average irradiation value of 800 W/m² was used, consistent with common practices in reputable publications [18]. Calculations were based on a steady-state system independent of time, a standard approach for such analyses. Parabolic trough collectors (PTCs) are employed to harness solar energy. The planned installation site has an area of 50,000 m², and an appropriate number of collectors has been selected for this site. Each PTC measures 25 m by 5 m, with the system comprising 200 parallel flow groups, each containing two serial collectors. This configuration enables the achievement of high temperatures necessary for electricity generation. The working principle of PTCs involves concentrating solar energy to reach elevated temperatures. In the system, Therminol VP-1 is used as the heat transfer fluid (HTF), which is heated by the concentrated solar energy. The high-temperature fluid then transfers its heat to an ORC via a heat exchanger, enabling electricity generation. The ORC employs R-134a as the working fluid and consists of a pump, a heat exchanger, a turbine, and a condenser. R134a is a working fluid frequently used within the temperature ranges of this study. Alternative fluid selections can also be explored in a separate study [18]. Each component is modeled as a control volume under the open system assumption. The isentropic efficiencies of the turbine and pump are both assumed to be 85%. The dead state conditions, representing ambient reference values, are defined as 100 kPa and 298 K, with the subscript "0" used for notation. In this study, the system's energy and exergy efficiencies were calculated, and the system was optimized using a multi-objective optimization algorithm. Since solar irradiation was assumed to be constant, the optimization primarily focused on the ORC. The objectives included minimizing cost while maximizing net energy and exergy efficiencies. The optimization variables were the ORC turbine inlet pressure and mass flow rate.

2.2 Thermal Analysis of PTC

The maximum energy is obtained with a PTC collector is the total amount of irradiation per unit area (Eq. (1))[18].

$$Q_{in} = I \cdot A_{tot} \quad (1)$$

Only a certain part of this energy is converted into useful energy. This converted energy can be measured from the difference between the inlet and outlet water temperatures:

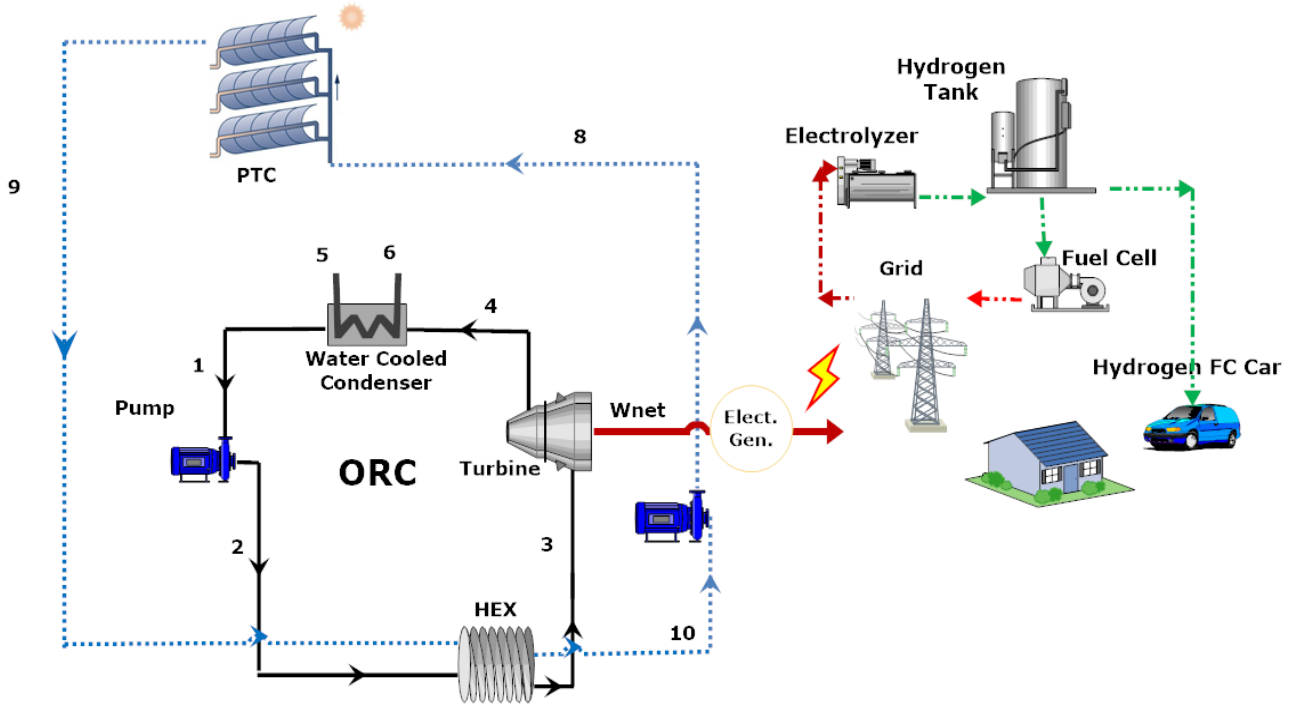


Figure 1. Schematic representation of the modeled system.

$$Q_u = \dot{m}_{tot} \cdot C_{p,hf} \cdot (T_{hf,out} - T_{hf,in}) \quad (2)$$

However, it is more difficult to calculate and estimate without knowing the exit temperature. For this, it is necessary to determine the losses from the collected energy. First of all, there is the concept of optical efficiency, only a part of the incoming energy can be optically focused and absorbed by the surfaces [19]. It shown in Eq. (3)

$$Q_{abs} = Q_{in} \cdot \eta_{optical} \quad (3)$$

The optical efficiency term encompasses various factors such as transmittance, reflectance, and absorbance [20]. In this study, these factors are not detailed individually. The receiver's optical efficiency is taken as 0.806 (or 80.6%), which aligns with values reported in the literature [19].

Following optical losses, thermal losses also occur and can be analyzed as heat flow within the pipe. Determining these thermal losses requires knowledge of the surface temperatures. The analysis involves examining the heat transfer between surfaces step by step. First, heat transfer occurs between the liquid inside the pipe and the pipe wall. To quantify this, the flow characteristics within the pipe and the Nusselt number (Nu) are calculated. This step yields the useful heat transfer. Next, heat transfer occurs between the outer surface of the pipe and the glass cover. Finally, another heat transfer takes place between the glass cover and the sky or surrounding air. The heat fluxes for these thermal losses are equal, and the surface temperatures of the components are interdependent. Using an iterative approach, the heat

fluxes are balanced, allowing the unknown surface temperatures to be estimated. The final, precise values are obtained after several iterations.

The outermost layer involves heat transfer between the glass cover and the sky. In this process, convection from the cover to the air and irradiation from the cover to the sky are considered. These two mechanisms are expressed as a combined heat transfer in Eq. (4) [21]. Sky temperature is Eq. (5) [22];

$$Q_{loss} = A_{co} \cdot h_{amb} \cdot (T_c - T_{amb}) + A_{co} \cdot \sigma \cdot \epsilon_c \cdot (T_c^4 - T_{sky}^4) \quad (4)$$

$$T_{sky} = 0.0553 \cdot T_{amb}^{1.5} \quad (5)$$

The thermal convection coefficient of air can be found by using Nusselt correlations in Eq.(6) [19].

$$Nu_{amb} = 0.193 \cdot Re_{amb}^{0.618} \cdot Pr_{amb}^{0.33} \quad (6)$$

To calculate the Nusselt number, the Reynolds number from Eq. (7) is substituted into Eq. (6). Subsequently, the convection coefficient is determined by substituting the Nusselt number into Eq. (8) [23];

$$Re_{amb} = \frac{u_{amb} \cdot D_{co}}{\nu_{amb}} \quad (7)$$

$$Nu_{amb} = \frac{h_{amb} \cdot D_{co}}{k_{amb}} \quad (8)$$

In the same way, another heat transfer surface occurs between the cover and the tube. Since this area is vacuum, only irradiation is involved and this showed in Eq. (9) [24].

$$Q_{loss} = \frac{A_{ro} \cdot \sigma \cdot (T_r^4 - T_c^4)}{\frac{1}{\varepsilon_r} + \frac{1 - \varepsilon_c}{\varepsilon_c} \cdot \left(\frac{A_{ro}}{A_{ci}} \right)} \quad (9)$$

The heat transfer between the flow in the innermost tube also occurs only as convection. The flow in the tube can be solved with the heat transfer model [24];

$$Q_u = A_{ri} \cdot h_{hf} \cdot (T_r - T_{hf,m}) \quad (10)$$

Total energy balance is;

$$Q_{abs} = Q_u + Q_{loss} \quad (11)$$

After finding the useful heat, the solar energy output temperature can be found. Thus, the temperature of the HTF that heats the ORC cycle has been determined.

2.3 Thermodynamic analysis of ORC

The cycle is then analyzed. There is a heat exchanger turbine, pump and condenser in the cycle. The energy and exergy balance of these systems is given in Table 1[25].

2.4 Economic Analysis

The interest value and future value of money are calculated according to Equations (12-15) [26];

$$F = P(1+i)^n \quad (12)$$

$$F = P \left(1 + \frac{i}{p} \right)^{np} \quad (13)$$

$$i_{eff} = \left(1 + \frac{i}{p} \right)^p - 1 \quad (14)$$

$$F = P(1 + ni_{eff}) \quad (15)$$

The "cost recovery factor" (CRF) is calculated according to its lifetime and interest rate in Eq. (16) [26] to calculate the annual recovery of a cost.

$$CRF = \frac{A}{P} = \frac{i_{eff} (1 + i_{eff})^n}{(1 + i_{eff})^n - 1} \quad (16)$$

If the annual levelized investment cost of the component is calculated from here, Eq. (17) is obtained [26].

$$\dot{Z}_c^{IC} = \frac{CRF}{\tau} C_c \cdot (1 + r_n)^2 \quad (17)$$

In addition to the annual levelized investment cost of the component, maintenance, and operating costs will also be included. If these costs are included, the total cost will be Eq. (18).

$$\dot{Z}_c = \dot{Z}_c^{IC} + \dot{Z}_c^M \quad (18)$$

Maintenance operating costs vary depending on the component. It is shown in Eq. (19).

$$\dot{Z}_c^M = \frac{CRF \cdot C_{L,M}}{\tau} \frac{C_c}{\sum_k C_c} \quad (19)$$

Up to this point, only the cost of the component has been examined, its annual levelized cost. However, the system produces energy and actively each unit of energy flow or change has a cost to the system. In short, if all these changes are shown as exergy and the cost of each exergy change is calculated, the cost of each unit of exergy or the product produced on the system can also be found. This method is called the SPECO method [26].

The sum of the exergy and levelized cost of the components entering the system constitutes the cost of the products coming out. This can be shown mathematically as;

$$\dot{C}_{P,tot} = \dot{C}_{F,tot} + \dot{Z}_{tot}^{IC} + \dot{Z}_{tot}^M \quad (20)$$

2.5 Hydrogen Technology

Hydrogen has been a highly researched topic in recent years, serving as a critical technology for energy storage and transportation [27]. Using fuel cells, chemical energy can be converted into electrical energy, enabling hydrogen-powered electric vehicles to become a reality. In addition to its utilization, the production of hydrogen is equally important. While fossil fuel-based reforming remains a common method, electrolysis powered by renewable energy sources is gaining significance. Electrolyzers, as key hydrogen production mechanisms, are still under development and expected to see broader adoption in the future [28]. In this study, an electrolyzer and a fuel cell were incorporated into the model to simulate hydrogen production and utilization.

The modeling was conducted from a purely thermodynamic perspective, and the corresponding analyses and models are presented in Table 1. The efficiencies of the electrolyzer and fuel cell were assumed to be 70%. Although this value is below the theoretical upper limit of 83-85%, it aligns well with practical data commonly reported in the

literature [29, 30]. Although some studies use lower values, the highest practical values found in the literature were preferred in this study to better align with future projections. Additionally, the efficiencies of these systems are influenced

by factors such as operating conditions, environmental impacts, and system scale. These factors can involve highly detailed analyses within their own scope.

Table 1. Thermodynamic behavior of the system components

Pump	Conservation of Mass	$\dot{m}_1 = \dot{m}_2$
	Energy Balance	$\dot{W}_p = \dot{m}v_1(P_2 - P_1) / \eta_p$ $\eta_p = \frac{W_{p,rev}}{W_p}$
	Exergy Balance	$\dot{E}x_{dest} = W_p - W_{p,rev}$
Turbine	Conservation of Mass	$\dot{m}_1 = \dot{m}_2$
	Energy Balance	$\dot{W}_{turb} = \dot{m}_1(h_1 - h_2)$ $\eta_{turb} = \frac{h_1 - h_2}{h_1 - h_{2,s}}$
	Exergy Balance	$\dot{E}x_{dest} = \dot{W}_{turb,rev} - \dot{W}_{turb}$
Heat Exchanger	Conservation of Mass	$\dot{m}_{c,g} = \dot{m}_{c,\zeta}$ $\dot{m}_{h1,g} = \dot{m}_{h1,\zeta}$ $\dot{m}_{h2,g} = \dot{m}_{h2,\zeta}$
	Energy Balance	$\dot{m}_{h1,i}(h_{h,i} - h_{h,e}) = \dot{m}_{c,i}(h_{c,e} - h_{c,i})$
	Exergy Balance	$\dot{E}x_{dest} = \dot{m}_{h,i}(ex_{h,i} - ex_{h,e}) - \dot{m}_{c,i}(ex_{c,e} - ex_{c,i})$
Water Cooled Condenser	Conservation of Mass	$\dot{m}_{cool,i} = \dot{m}_{cool,e}$ $\dot{m}_i = \dot{m}_e$
	Energy Balance	$\dot{m}_{cool,i}(h_{cool,e} - h_{cool,i}) = \dot{m}_i(h_i - h_e)$
	Exergy Balance	$\dot{E}x_{dest} = \dot{m}_{cool,i}(ex_{cool,e} - ex_{cool,i}) - \dot{m}_i(ex_i - ex_e)$
PTC	Conservation of Mass	$\dot{m}_i = \dot{m}_e$
	Energy Balance	$\dot{Q}_{solar,g} = N.I.A_{col}$ $\eta_{solar} = \frac{\dot{Q}_u}{\dot{Q}_{solar,g}}$
	Exergy Balance	$\dot{E}x_{solar,in} = \dot{Q}_{solar,g} \left[1 + 0.33 \left(\frac{T_0}{T_{solar}} \right)^4 - \frac{4}{3} \left(\frac{T_0}{T_{solar}} \right) \right]$ $\dot{E}x_{dest} = \dot{E}x_{solar,in} - \dot{m}_i(ex_e - ex_i)$
Electrolyzer	Conservation of Mass	$\dot{m}_{H_2O} = \dot{m}_{H_2} + \dot{m}_{O_2}$
	Energy Balance	$\eta_{Electrolyzer} = \frac{LHV_{H_2} \cdot \dot{m}_{H_2}}{\dot{W}_{in,Electrolyzer}}$
	Exergy Balance	$\dot{E}x_{dest} = \dot{W}_{in} - \dot{E}x_{H_2}$
Fuel Cell	Conservation of Mass	$\dot{m}_{H_2} + \dot{m}_{O_2(Air)} = \dot{m}_{H_2O}$
	Energy Balance	$\eta_{FC} = \frac{\dot{W}_{out,FC}}{LHV_{H_2} \cdot \dot{m}_{H_2}}$
	Exergy Balance	$\dot{E}x_{dest} = \dot{E}x_{H_2} - \dot{W}_{out}$

2.6 Multi-objective Optimization

Optimization plays a crucial role in many engineering applications [31,32]. In this study, optimization is performed based on cost, net work output, and exergy efficiency. To integrate these objectives, a multi-objective optimization algorithm was developed, allowing the simultaneous optimization of multiple variables[33]. A graphical approach was employed to facilitate this process, allowing different functions to be represented on a common graph. Initially, the variation range of the cost function was plotted. The minimum point on this graph, representing the optimal cost, was assigned a value of 1. Conversely, the maximum cost, representing the worst-case scenario, was assigned a value of 0. This normalization process is mathematically expressed using the normalization algorithm provided in Eq. (21).

$$1 - \frac{C_n - C_{min}}{C_{min_{max}}} \quad (21)$$

The same process was applied to net work output and efficiency term, aiming for maximization. Values within the selected range were calculated, with the highest marked as "1" and the lowest as "0." Normalization was performed accordingly in Eq. (22) and Eq. (23).

$$1 - \frac{W_{max} - W_n}{W_{max} - W_{min}} \quad (22)$$

$$1 - \frac{\eta_{ex,max} - \eta_{ex,n}}{\eta_{ex,max} - \eta_{ex,min}} \quad (23)$$

After completing these operations, the net work output, cost, and efficiency were transformed into three normalized functions ranging between 0 and 1. A common objective function was then created graphically. Since this study involves three objectives, a weight coefficient was assigned to each, with their sum equaling 1. If all objectives are equally important, the weights are set to 1/3, 1/3, 1/3. However, if cost is prioritized over net work output, its coefficient is assigned a value greater than 1/3, while the other coefficients adjust to maintain the total sum of 1 (e.g., 0.4, 0.3, and 0.3, or 0.2, 0.3, and 0.5). Similarly, if net work output or efficiency is prioritized, their respective coefficients are increased. The resulting combined objective function is expressed in Eq. (24).

$$A_0 = a_1 \left(1 - \frac{W_{max} - W_n}{W_{max} - W_{min}} \right) + a_2 \left(1 - \frac{C_n - C_{min}}{C_{max} - C_{min}} \right) + a_3 \left(1 - \frac{\eta_{ex,max} - \eta_{ex,n}}{\eta_{ex,max} - \eta_{ex,min}} \right) \quad (24)$$

$$a_1 + a_2 + a_3 = 1$$

3. Results

Performing an energy analysis of the system reveals the amount of net power it can generate. Net power production depends on various parameters of the system. Some of these factors are external, such as the amount of solar energy, which cannot be altered by operators. However, there are also operating and design variables that affect the performance of the system. Particularly in the case of the ORC cycle, altering system parameters significantly affects energy efficiency. The T-s diagram of the ORC cycle for the base case scenario is provided in Figure 2. The turbine inlet pressure is 3500 kPa, and the condenser inlet pressure is 780 kPa. The critical pressure is 4000 kPa, which has been set as the upper limit for optimization. At a solar irradiation level of 800 W/m², the solar energy system reaches a maximum temperature of 441 K. When this thermal energy is transferred to R-134a through the heat exchanger, the ORC system achieves a maximum temperature of 417 K. The minimum temperature in the ORC system is evaluated at the condenser outlet, calculated as 303 K. The turbine inlet pressure and the mass flow rate of the working fluid are significant variables influencing the system's outputs, making them the selected parameters for optimization.

First parameter is the turbine inlet pressure. Increasing this pressure at certain rates can increase system performance. Again, the mass flow rate of the fluid in the system is also effective on system performance. These two variables also influence the system's costs. The variations in mass flow rate and net energy output in the ORC were analyzed at a constant pressure, as shown in Figure 3. In this graph, the net energy output reaches its maximum at a mass flow rate of 42 kg/s. This represents the optimal point where the energy transferred in the heat exchanger is most effectively absorbed by the working fluid.

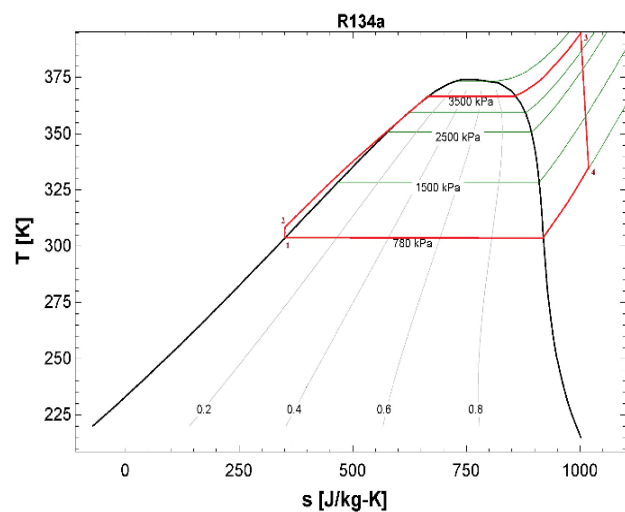


Figure 2. ORC diagram on the T-s graph of R134-a

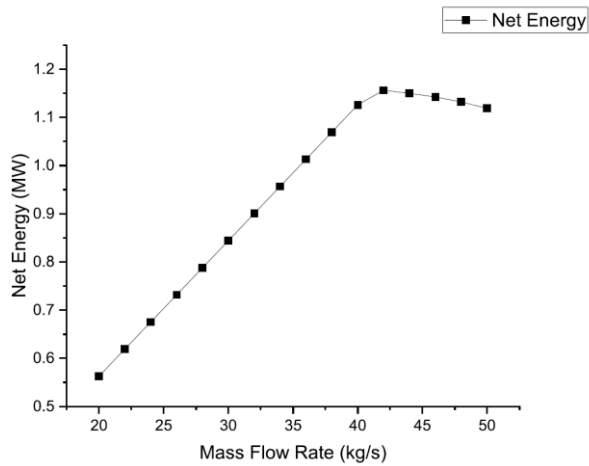


Figure 3. Produced net energy vs. mass flow rate

the pressure increases.

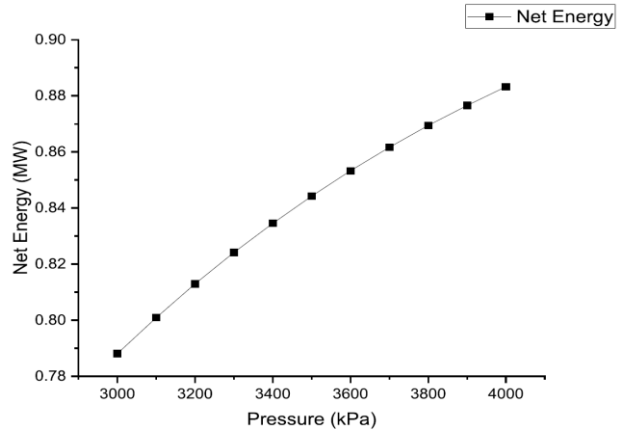


Figure 5. Produced net energy vs. turbine pressure

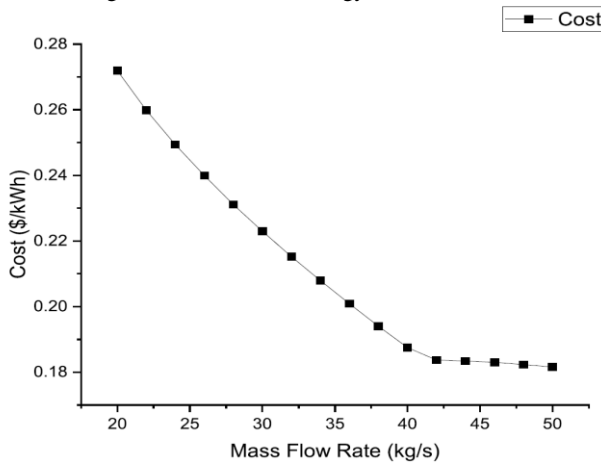


Figure 4. Unit cost of energy vs. mass flow rate

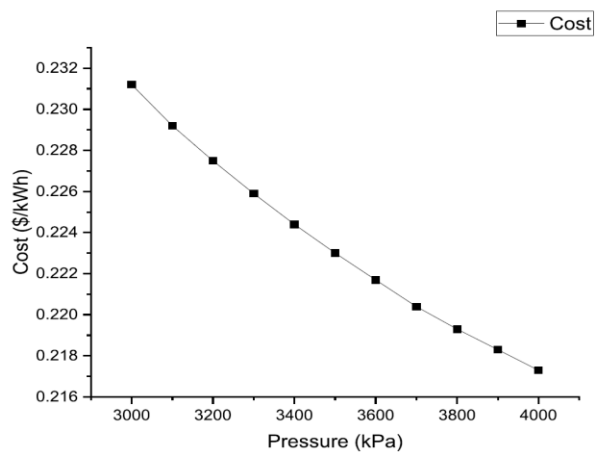


Figure 6. Unit cost of energy vs. turbine pressure

Similarly, when mass flow rate and cost are examined alone, there is a cost that decreases with increasing mass flow rate in Figure 4. However, this decrease is not linear. After the value of 42 kg/s the decreasing trend is getting lower. The lowest cost is at 50 kg/s.

In the previous graphs, the pressure was held constant. Comparable results were observed when varying the pressure while maintaining a constant mass flow rate, aligned with the base case scenario. Figure 5. illustrates how changes in pressure affect the net energy output. The net energy exhibits a polynomial trend, with diminishing growth as pressure increases. It peaks at 4000 kPa, the upper limit of the studied range. Although the curve might reach a maximum beyond 4000 kPa, such values were excluded from the study due to the onset of supercritical conditions. While systems operating above critical pressure do exist, a more detailed analysis of the system would be required for such scenarios.

An economic analysis was conducted with a base case system flow rate of 30 kg/s, as depicted in Figure 6. A unit energy cost curve was generated by varying the mass flow rate. The results indicate that unit energy cost decreases as

There are two variables, and the system responds differently to changes in each. To analyze their effects, it is crucial to present all outcomes in a single graph. The net work produced by the system was selected as the evaluation criterion, and a graph was created accordingly. This variation is displayed in a three-dimensional graph in Figure 7. The maximum net work was achieved when the mass flow rate approached 42 kg/s, and the turbine inlet pressure reached 4000 kPa.

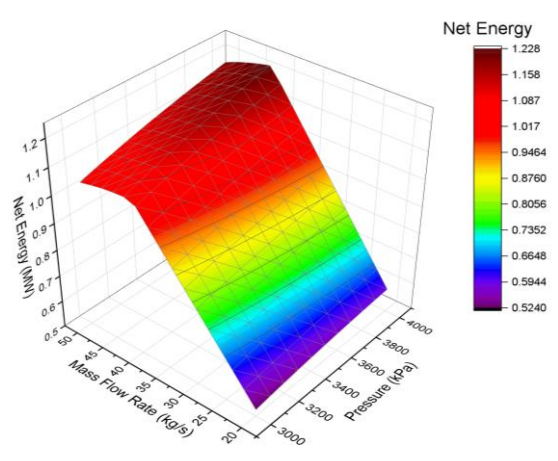


Figure 7. Net energy vs. pressure and mass flow rate

Similarly, the cost function can be represented with two parameters, as shown in Figure 8. The lowest cost is observed at 50 kg/s and 4000 kPa. It is important to note that the parameters minimizing cost differ from those maximizing work output. Therefore, it would be more appropriate to evaluate these values using a multi-objective optimization algorithm.

Additionally, when examining exergy efficiency, it can be observed that it follows a trend parallel to the net work output, as shown in Figure 9. The maximum efficiency was again calculated at 42 kg/s and 4000 kPa. Since the system's sole work output is derived from the ORC, it is logical for these values to align. However, in more complex systems that may be designed in the future, these values could differ.

Finally, the system is optimized, and values generated using a unified objective function are obtained (Figure 10.). These values range between zero and one. The expected optimum point lies between the parameters that directly maximize work output and those that minimize cost.

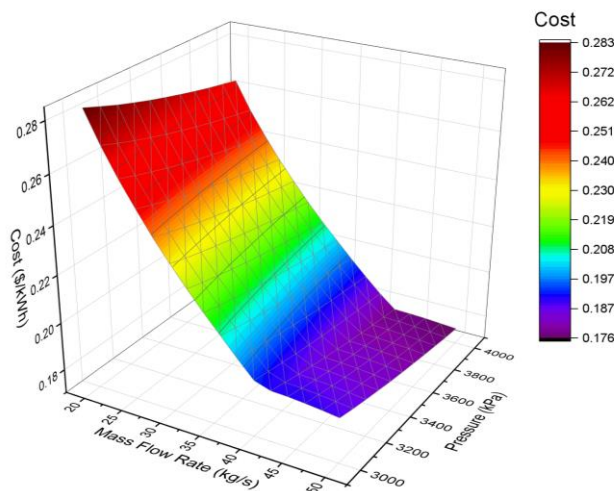


Figure 8. Unit cost vs. pressure and mass flow rate

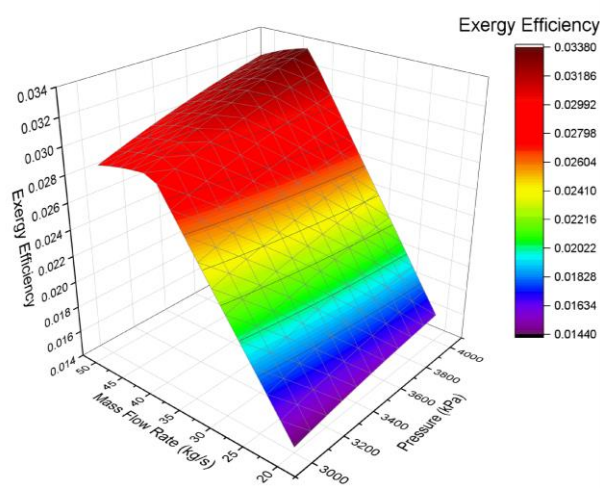


Figure 9. Exergy efficiency vs. pressure and mass flow rate

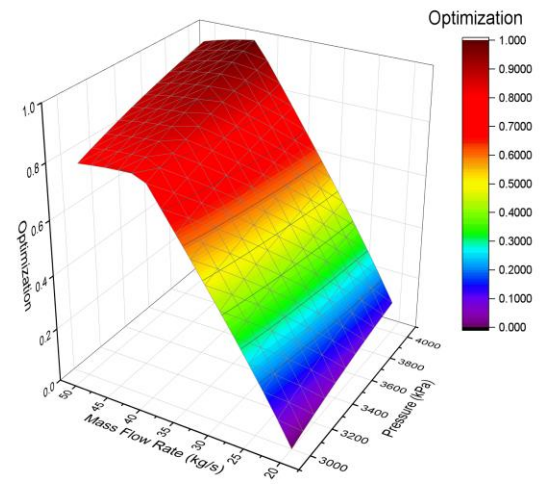


Figure 10. Optimization function vs. pressure and mass flow rate

However, the most accurate result is achieved through weighted and normalized multi-objective optimization. Interestingly, the optimum point aligns with the one that maximizes work output. This is because, upon examining the cost graph independently, although the lowest cost is observed at 50 kg/s, the change beyond 42 kg/s is negligible. Therefore, the optimum point is determined as 42 kg/s and 4000 kPa through the multi-objective optimization algorithm.

The optimum point was compared with the base case scenario used in the initial calculation. In the first calculation, the mass flow rate and pressure were assumed constant at 30 kg/s and 3500 kPa, respectively. Following the optimization, the most optimum values were determined to be 42 kg/s and 4000 kPa. A comparison of these values is presented in Table 2. Additionally, the energy storage capacity of the system was evaluated. The table illustrates the amount of hydrogen produced when the electrolyzer and fuel cell storage are utilized, as well as the amount of energy released when this hydrogen is reconverted into energy. The hydrogen produced can be used for various purposes. These purposes are also shown in Figure 1. These could include industrial facilities or hydrogen-powered vehicles, which are expected to become more widespread in the future. The purpose here is to explain the production cost and quantity of hydrogen from PTC solar energy plant. Hydrogen is an important tool in energy storage and storage is important for renewable sources. Also in this table, the unit energy cost for the optimum case is calculated as 0.1781 \$/kWh. This value may be considered high in terms of cost, but it is consistent with the scope of this study, which focuses solely on electricity generation. The energy obtained from solar energy systems is generally more costly compared to other sources. Similar figures have also been found in the literature. In a similar study, Desai and Bandyopadhyay [10] reached a value of 0.188 \$/kWh. One way to reduce this value is by transforming the system into a multigeneration system with different aims and functions (such as heating ,cooling etc.).

Table 2. Base case and optimum case results

	Base Case	Optimum Case	Difference	% Change
Solar Irradiation	800 W/m ²	800 W/m ²	-	-
Area	5000 m ²	5000 m ²	-	-
High Pressure	3500 kPa	4000 kPa	500 kPa	14.30%
Mass Flow Rate in ORC	30 kg/s	42 kg/s	12 kg/s	40%
Net Energy	0.8443 MW	1.2280 MW	0.3837MW	45.45%
Exergy Efficiency	2.32%	3.37%	1.02	45.45%
Unit Cost of Energy	0.2230 \$/kWh	0.1781 \$/kWh	0.0449\$/kWh	20.13%
Hydrogen Production Rate	0.005023 kg/s	0.007307 kg/s	0.002284	45.45%
Fuel Cell Electric Rate	0.42 MW	0.61 MW	0.19 MW	45.45%

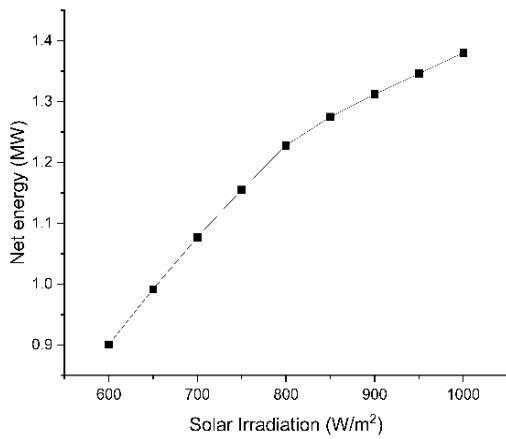


Figure 9. Graph of net energy change with varying solar irradiation

The solar irradiation value fluctuates throughout the day and cannot be controlled or optimized by operators. While a detailed discussion on this topic is beyond the scope of this work, the effect of solar irradiation in the final optimized case is briefly presented as a parametric result to guide researchers. As expected, net energy production increases with the rise in solar irradiation. This increase follows a parabolic curve with diminishing returns, suggesting that not all of the intense solar energy can be utilized efficiently. As the irradiation value increases, temperatures also rise, leading to greater temperature differences and, as a result, higher heat losses.

3. Conclusions

In conclusion, it is crucial to design renewable energy systems that can meet the rapidly growing energy demand. However, it is not enough to simply increase the number of renewable plants; ensuring that they operate efficiently is also essential. Each system has its own dynamics, and it is

not feasible to model and optimize all systems using a single equation. The energies entering and exiting the system, along with other variables, significantly impact the results. In this study, two key variables mass flow rate and turbine inlet pressure were altered, and various system outputs were examined. These common outputs were then optimized using a single function. As a result of the optimization, both efficiency and net work increased by approximately 45%, while unit energy cost decreased by about 20%.

Another important point to address is the cost of energy. A value of 0.22 \$/kWh, or even 0.18 \$/kWh when optimized, is quite high. The reason for the high cost is that the study is designed solely for electricity generation. Additionally, energy efficiency is quite low. Integrating functions such as heating, cooling, and other multigeneration applications would enhance system efficiency. This, in turn, could also lead to a reduction in costs. For example, a portion of the system's waste heat can be used for heating during the winter months. Alternatively, the system can be adjusted to operate more efficiently by integrating with other sources. However, the aim of the current study is to increase the system's efficiency by changing parameters within the system itself, rather than through external interventions. A simple system design has been used to observe the results and confirm the efficiency of the optimization method. Of course, in later stages and future studies, this method can be applied to more complex systems, and additional sources can be integrated into the existing PTC. Energy can also be used for different purposes.

The importance of multi-objective optimization studies in these systems is growing. This study demonstrated that this method is a reliable optimization algorithm that provides useful results. In future research, more complex systems can be optimized, leading to higher efficiencies and lower costs.

Declaration

The author declared no potential conflicts of interest with respect to the research, authorship, and/or publication of this article. The author also declared that this article is original, was prepared in accordance with international publication and research ethics, and ethical committee permission or any special permission is not required.

Author Contributions

Ömer Faruk Güler developed the model, performed calculations, optimized the system and wrote the manuscript.

Nomenclature

- A : Area
- a : Weight of parameter
- An : Annual
- C : Cost
- CRF : Cost Recovery Factor

D	: Diameter
F	: Future value
HTF	: Heat transfer fluid
h_n	: Enthalpy
h	: Convection coefficient
I	: Solar irradiation
i	: Inflation rate
LHV	: Lower Heating Value
\dot{m}	: Mass flow rate
N	: Number of collectors
Nu	: Nusselt Number
ORC	: Organic Rankine cycle
P	: Present value
Pr	: Prandtl Number
PTC	: Parabolic trough collector
Q	: Heat
Re	: Reynolds Number
SPECO	: Specific exergy cost
T	: Temperature
\dot{W}	: Work
Z	: Total cost rate
ε	: Emittance
σ	: Stefan-Boltzman Number
τ	: Annual operating time
amb	: Ambient
c	: Component
co	: Cover Outlet
col	: Collector
cool	: Cooling water
dest	: Destruction
e	: Exit
eff	: Effective
H ₂	: Hydrogen
htf	: Heat Transfer Fluid
in	: Inlet
max	: Maximum
min	: Minimum
n	: Number
out	: Outlet
p	: Pump
r	: Receiver
sky	: Sky
tot	: Total
turb	: Turbine
u	: Useful
IC	: Investment cost
M	: Maintenance

References

1. Teevan, C., Medinilla, A., & Sergejeff, K., The Green Deal in EU foreign and development policy, 2021. ECDPM Briefing Note, p. 131.
2. Gharat, P. V., Bhalekar, S. S., Dalvi, V. H., Panse, S. V., Deshmukh, S. P., & Joshi, J. B., Chronological development of innovations in reflector systems of parabolic trough solar collector (PTC)-A review. *Renewable and Sustainable Energy Reviews*, 2021. **145**: p. 111002.
3. Ghazouani, M., Bouya, M., & Benaissa, M., Thermo-economic and exergy analysis and optimization of small PTC collectors for solar heat integration in industrial processes. *Renewable Energy*, 2020. **152**: p. 984-998.
4. Park, J., Kang, S., Kim, S., Cho, H. S., Heo, S., & Lee, J. H., Techno-economic analysis of solar powered green hydrogen system based on multi-objective optimization of economics and productivity. *Energy Conversion and Management*, 2024. **299**: p. 117823.
5. Liu, L., Zhai, R., Xu, Y., Hu, Y., Liu, S., & Yang, L., Comprehensive sustainability assessment and multi-objective optimization of a novel renewable energy driven multi-energy supply system. *Applied Thermal Engineering*, 2024. **236**: p. 121461.
6. Fu, L., Fan, J., Yuanchun, L., Yantao, T., & Yisong, D., Study and application of a constrained multi-objective optimization algorithm. In *Proceedings of the IEEE International Vehicle Electronics Conference*, 1999. (IVEC'99)(Cat. No. 99EX257) p. 305-307
7. Yilmaz, F., An innovative study on a geothermal based multigeneration plant with transcritical CO₂ cycle: Thermodynamic evaluation and multi-objective optimization. *Process Safety and Environmental Protection*, 2024. **185**: p. 127-142.
8. Li, C., & Zhai, R., A novel solar tower assisted pulverized coal power system considering solar energy cascade utilization: Performance analysis and multi-objective optimization. *Renewable Energy*, 2024. **222**:119891.
9. Tian, Y., Cheng, R., Zhang, X., & Jin, Y., PlatEMO: A MATLAB platform for evolutionary multi-objective optimization [educational forum]. *IEEE Computational Intelligence Magazine*, 2017. **12**(4): p. 73-87.
10. Desai, N. B., & Bandyopadhyay, S., Optimization of concentrating solar thermal power plant based on parabolic trough collector. *Journal of Cleaner Production*, 2015. **89**: p. 262-271.
11. Babaelahi, M., Mofidipour, E., & Rafat, E., Combined Energy-Exergy-Control (CEEC) analysis and multi-objective optimization of parabolic trough solar collector powered steam power plant. *Energy*, 2020. **201**: p. 117641.
12. Colakoglu, M., & Durmayaz, A., Energy, exergy and environmental-based design and multiobjective optimization of a novel solar-driven multi-generation system. *Energy Conversion and Management*, 2021. **227**: p. 113603.
13. Georgousis, N., Lykas, P., Bellos, E., & Tzivanidis, C., Multi-objective optimization of a solar-driven polygeneration system based on CO₂ working fluid. *Energy Conversion and Management*, 2022. **252**: p. 115136.
14. Modabber, H. V., & Manesh, M. H. K., Optimal exergetic, exergoeconomic and exergoenvironmental design of polygeneration system based on gas Turbine-Absorption Chiller-Solar parabolic trough collector units integrated with multi-effect desalination-thermal vapor compressor-reverse osmosis desalination systems. *Renewable Energy*, 2021. **165**: p. 533-552.
15. Esfahani, M. N., Aghdam, A. H., & Refahi, A., Energy, exergy, exergoeconomic, exergoenvironmental (4E) assesment, sensitivity analysis and multi-objective optimization of a PTC-tehran climate data case study. *Journal of Cleaner Production*, 2023. **415**: p. 137821.
16. Adun, H., Adedeji, M., Adebayo, V., Shefik, A., Bamisile, O., Kavaz, D., & Dagbasi, M., Multi-objective optimization and energy/exergy analysis of a ternary nanofluid based parabolic trough solar collector integrated with kalina cycle. *Solar Energy Materials and Solar Cells*, 2021. **231**: p. 111322.

17. Hocaoglu, F. O., & Serttas, F., A novel hybrid (Mycielski-Markov) model for hourly solar radiation forecasting. *Renewable Energy*, 2017. **108**: p. 635-643.
18. Guler, O. F., Sen, O., Yilmaz, C., & Kanoglu, M., Performance evaluation of a geothermal and solar-based multigeneration system and comparison with alternative case studies: Energy, exergy, and exergoeconomic aspects. *Renewable Energy*, 2022. **200**: p. 1517-1532.
19. Bellos, E., & Tzivanidis, C., A detailed exergetic analysis of parabolic trough collectors. *Energy Conversion and Management*, 2017. **149**: p. 275-292.
20. Behar, O., Khellaf, A., & Mohammedi, K., A novel parabolic trough solar collector model–Validation with experimental data and comparison to Engineering Equation Solver (EES). *Energy Conversion and Management*, 2015. **106**: p 268-281.
21. Ferraro, V., Imineo, F., & Marinelli, V., An improved model to evaluate thermodynamic solar plants with cylindrical parabolic collectors and air turbine engines in open Joule–Brayton cycle. *Energy*, 2013. **53**: p. 323-331.
22. Swinbank, W. C., Long-wave radiation from clear skies. *Quarterly Journal of the Royal Meteorological Society*, 2013. **89**(381): p. 339-348.
23. Kakaç, S., Liu, H., & Pramuanjaroenkij, A., *Heat exchangers: selection, rating, and thermal design*. CRC press, 2012. p. 81-128
24. Bellos, E., Tzivanidis, C., & Antonopoulos, K. A., A detailed working fluid investigation for solar parabolic trough collectors. *Applied Thermal Engineering*, 2017. **114**: p. 374-386.
25. Sen, O., Guler, O. F., Yilmaz, C., & Kanoglu, M., Thermodynamic modeling and analysis of a solar and geothermal assisted multi-generation energy system. *Energy Conversion and Management*, 2021. **239**: p. 114186.
26. Bejan, A., Tsatsaronis, G., & Moran, M. J., *Thermal design and optimization*. 1995, USA: John Wiley & Sons.
27. Miri, M., Tolj, I., & Barbir, F., Review of Proton Exchange Membrane Fuel Cell-Powered Systems for Stationary Applications Using Renewable Energy Sources. *Energies*, 2024. **17**(15): p. 3814.
28. Alkhalidi, S. A., & Prasad, A. K., Strategies for gas management in the PEM water electrolyzer anode. *Journal of Power Sources*, 2025. **626**: p. 235747.
29. Astriani, Y., Tushar, W., & Nadarajah, M., Optimal planning of renewable energy park for green hydrogen production using detailed cost and efficiency curves of PEM electrolyzer. *International Journal of Hydrogen Energy*, 2024. **79**: p. 1331-1346.
30. Larminie, J., & Dicks, A., *Fuel cell systems explained* (2nd ed.). 2003, England: John Wiley & Sons.
31. Yilmaz, C., Cengiz, E., & Kahraman, H. T., A new evolutionary optimization algorithm with hybrid guidance mechanism for truck-multi drone delivery system. *Expert Systems with Applications*, 2024. **245**: p. 123115.
32. Şeker, M., Mutlu, İ., Aysal, F. E., Atli, I. S., Yavuz, I., & Ergün, Y. A., The ANN analysis and Taguchi method optimisation of the brake pad composition. *Emerging Materials Research*, 2021. **10**(3): p. 314-320.
33. Li, L., Liu, P., Li, Z., & Wang, X., A multi-objective optimization approach for selection of energy storage systems. *Computers & Chemical Engineering*, 2018. **115**: p. 213-225.